Colloid Polym Sci (2004) 282: 1258–1267
DOI 10.1007/s00396-004-1073-8

ORIGINAL CONTRIBUTION

Tz. Ivanova
I. Minkov
I. Panaiotov
P. Saulnier
J. E. Proust

Dilatational properties and morphology of surface films spread from clinically used lung surfactants

Received: 24 October 2004
Accepted: 4 February 2004
Published online: 5 March 2004

Tz. Ivanova (✉) · I. Minkov · I. Panaiotov
Biophysical Chemistry Laboratory,
University of Sofia, James Bourchier str. 1,
1126 Sofia, Bulgaria
E-mail: tzivanova@chem.uni-sofia.bg

P. Saulnier · J. E. Proust
Ingénierie de la Vectorisation Particulaire,
INSERM ERIT-M, Immeuble IBT,
10 rue A. Boquel, 49100 Angers, France

Abstract The dilatational properties, structure, and morphology of the surface films spread at the air–water interface from complex lipid/protein systems were studied by measuring the surface pressure–area and surface potential–area isotherms, the surface rheological properties, and AFM images. The commercially available lung surfactants Alveofact, Curosurf, Survanta, and Exosurf were used as examples. The isotherms of the studied lung surfactant surface films are compared with model lipid and protein monolayers spread from bulk solutions. On the basis of a simple rheological model, the values for the elasticity and the specific time of relaxation related to the reorganization processes occurring in the monolayers were calculated. The spread films of natural surfactants Curosurf and Alveofact show a high effectiveness of spreading and respreading under the conditions of this study. These observations were confirmed by AFM imaging.

Keywords Pulmonary surfactants · Surface rheology · Surface films · AFM imaging

Introduction

The spreading of small, variously organized structures containing lipids and proteins at biointerfaces and the consequent formation of surface films is often a step in many processes. A good example is the so-called lung surfactant.

It is now generally admitted [1, 2, 3, 4, 5, 6, 7, 8, 9, 10, 11] that a complex mixture of phospholipids, neutral lipids, and specific proteins is accumulated at the alveolar surface of the lungs. The surface-active molecules are synthesized in pneumocyte II, stored in lamellar bodies, and secreted via tubular myelin to the ''air–alveolar lining layer'' interface where a monolayer is formed. The usual criteria for favorable properties of the pulmonary surfactant are:

(i) Capacity of achieving low surface tension and high surface elasticity in order to contribute to maintaining the structural stability of the alveoli during their cyclic deformations accompanying respiration.
(ii) A high effectiveness in spreading of myelin structures and respreading of collapsed surfactant aggregates at the interface during respiration.
(iii) An appropriate state with a certain porosity and fluidity of the monolayer in relation to the gas exchange.

Commercially available surfactants are used clinically in the case of deficiency of pulmonary surfactant along with an immature structure of the lungs of neonates [12]. The main component present in the commercial surfactants—the saturated phospholipid DPPC (about 60–70% by weight in normal adults)—is capable of achieving near zero surface tension but its adsorption and respreading properties are poor. The idea that the hydrophobic surfactant-specific proteins SP-B and SP-C also present in the surfactants help to disrupt the phospholipid bilayers and aggregates, thereby facilitating the formation of the monolayer and respreading of the collapsed phase, was recently suggested [13, 14, 15, 16, 17]. The origin of

commercially available pulmonary surfactants (natural, seminatural or exogenous artificial), their composition (phospholipids, proteins, xenobiotics), and their tensioactive properties vary widely. An impressive body of papers is devoted to the surface properties of model and natural pulmonary monolayers [17, 18, 19, 20, 21].

The purpose of this paper is to study the mechanisms of spreading and dilatational properties of the surface films from complex lipid/protein systems. As an example four commercially available pulmonary surfactants, Alveofact, Curosurf, Survanta, and Exosurf, were used and their interfacial properties were compared with previously obtained data for model lipid/protein monolayers.

Materials and methods

Materials

1. Alveofact (Boehringer Ingelheim): Natural surfactant extract, prepared from bovine lung. A 1.2 ml suspension contains 50–60 mg phospholipid fraction (66 μmol mixed lipids), 5.4 mg (about 0.9%) NaCl, and a small amount of hydrophobic proteins SP-B and SP-C (about 1%).
2. Curosurf (Chiesi Farmaceutici, Parma, Italy): Natural surfactant extract, prepared from porcine lungs, containing almost exclusively polar lipids, in particular phosphatidylcholine (about 70% of total phospholipid content), phosphatidylglycerol (about 30% of total phospholipid content), and about 1% of hydrophobic proteins SP-B and SP-C. It is suspended in 0.9% sodium chloride solution. The pH is adjusted as required with sodium bicarbonate to a pH of 6.2 (5.5–6.5). Curosurf contains no preservatives.
3. Survanta Beractant (Ross Laboratories, Columbus, Ohio): Semisynthetic surfactant, one of the most commonly used in the USA. It is a natural extract of bovine lung surfactant, containing 88% phospholipids (about 50% dipalmitoylphosphatidylcholine) and contains the hydrophobic lung surfactant proteins (about 1%), supplemented with synthetic palmitic acid (PA) and tripalmitin (TP).
4. Exosurf Neonatal (Burroughs Wellcome, Research Triangle Park, NC, USA): Purely synthetic, protein-free surfactant preparation. It contains about 80% dipalmitoylphosphatidylcholine (DPPC) combined with hexadecanol and tyloxapol, added to partially overcome the bad spreading of DPPC. Exosurf contains no preservatives. Sodium hydroxide or hydrochloric acid may have been added to adjust pH. A disadvantage of Exosurf is related to the fact that hexadecanol and tyloxapol have no relation to natural lung surfactant.

NaCl is a product of Theokom (Sofia, Bulgaria). In all experiments double distilled water was used.

Methods

Measurement at the air–water interface

The pulmonary surfactant monolayers were formed by spreading the specified amounts of the solutions over the available area of a Teflon trough (180 cm^2) using an Exmire microsyringe. To be comparable with previously obtained data for model lipid and lipid/protein monolayers the temperature 22 ± 2 °C was chosen. The surface pressure (π) was measured using a KSV-2200 (Finland) surface balance equipped with a platinum plate. The surface potential (ΔV) was measured simultaneously by using a gold-coated ^{241}Am ionizing electrode, a reference electrode, and a KP 511 (Kriona, Bulgaria) electrometer, connected to a PC provided with user software for real-time data measurements. As usual, the surface potential of the pure aqueous surface fluctuated for about 30 min. The reproducibility of the initial surface potential value was ± 15 mV. When the air–water surface potential became constant, spreading of the monolayer was performed. After a new equilibration period of about 5–10 min, the surface potential became constant and the following three kinds of experiments were performed:

1. Surface pressure–area and surface potential–area isotherms were obtained after spreading on 0.14 M NaCl of various quantities from the studied pulmonary surfactant solutions. The monolayers were continuously compressed with a constant velocity $U_b = 10$ $cm^2.min^{-1}$.
2. Large surface pressure–area hysteresis cycles were obtained with $U_b = 10$ $cm^2.min^{-1}$ after spreading of various amounts of pulmonary surfactant solutions.
3. The rheological dilatational properties of the pulmonary surfactant monolayers were studied by measuring the surface pressure variations with time along the monolayer during and after a small continuous compression [17, 22, 23, 24, 25, 26, 27, 28, 29, 30, 31, 32]. The interpretation of the experimental data for the increase of the local surface pressure $\Delta\pi$ as a function of time at distance x is based on the rheological model shown in Fig. 1 [17]. The total surface pressure change $\Delta\pi = \pi(t) - \pi_i$ is represented as a sum of an equilibrium $\Delta\pi_e$ and a nonequilibrium $\Delta\pi_{ne}$ contribution:

$$\Delta\pi = \Delta\pi_e + \Delta\pi_{ne} \quad (1)$$

The equilibrium part $\Delta\pi_e$ (represented by the lower branch of the mechanical model) is related to the equilibrium surface dilatational elasticity E_e:

$$\Delta\pi_e = E_e \frac{U_b t}{A_i} \quad (2)$$

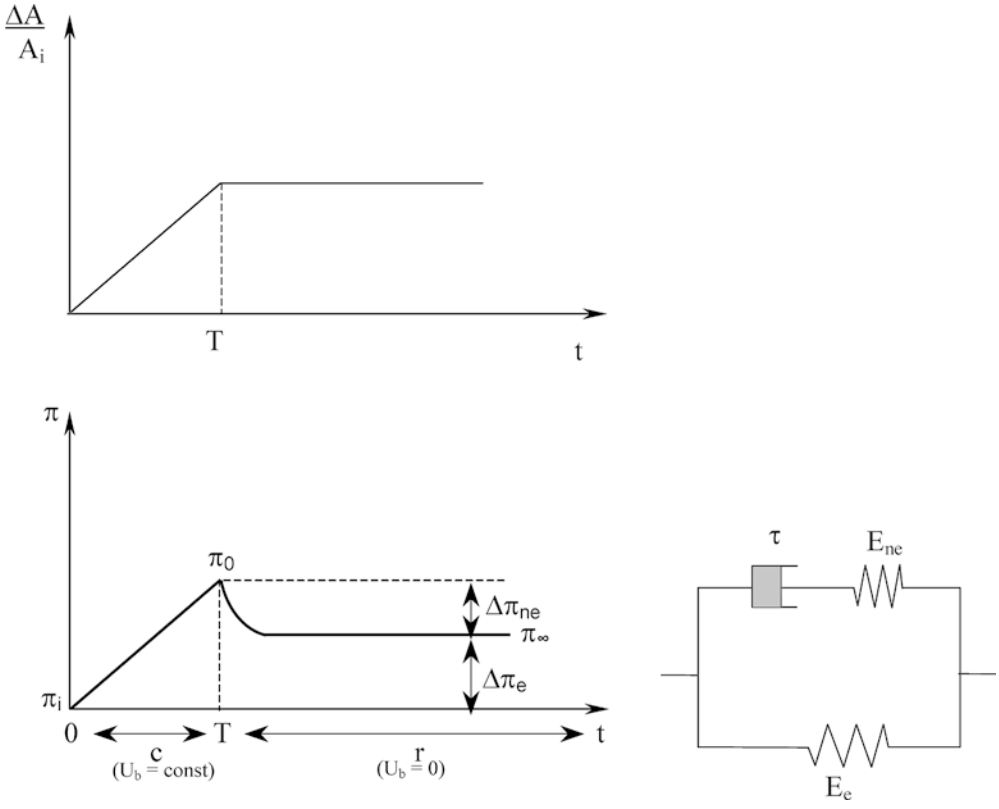

Fig. 1 Rheological model of the monolayer. Deformation $\Delta A/A_i \equiv U_b t/A_i$ and the change of surface pressure $\Delta\pi$ during the time T of compression c with constant velocity, followed by relaxation r with characteristic time τ. A_i and π_i are the initial surface area and surface pressure, respectively, before the compression; π_0 and π_∞ are the values of the surface pressure at the beginning and the end of relaxation, respectively. $\Delta\pi_e$ and $\Delta\pi_{ne}$ are the equilibrium and nonequilibrium parts of the total surface pressure change $\Delta\pi = \pi(t) - \pi_i$; E_e and E_{ne} are the equilibrium and nonequilibrium elasticities, respectively

where A_i is the initial surface area before the compression and $U_b t/A_i \equiv \Delta A/A_i$ is the corresponding strain (see Fig. 1).

The nonequilibrium part of the total surface pressure $\Delta\pi_{ne}$ (represented by the upper branch of the mechanical Maxwell's model) is associated with the accumulation of elastic energy during the compression and its dissipation through a specific molecular mechanism:

$$\frac{d\Delta\pi_{ne}}{dt} + \frac{\Delta\pi_{ne}}{\tau} = E_{ne}\frac{U_b}{A_i} \tag{3}$$

After integration of Eq. 3 the following expression describing the viscoelastic behavior of the monolayer is obtained [22]:

$$\frac{\Delta\pi}{U_b t}A_i = E_e + E_{ne}\frac{\tau}{t}\left(1 - e^{-\frac{t}{\tau}}\right) \tag{4}$$

At small time $t \ll \tau$, from Eq. 4 we obtain:

$$\frac{\Delta\pi}{U_b t}A_i = E_e + E_{ne} \tag{5}$$

The specific time of relaxation τ can be obtained from experiments with time of compression T much smaller than the time of the relaxation process τ ($T \ll \tau$):

$$\frac{\pi(t) - \pi_\infty}{\pi_0 - \pi_\infty} = e^{-\frac{t}{\tau}} \tag{6}$$

Atomic force microscopy

The Langmuir–Blodgett (LB) transfer was carried out on a freshly cleaved mica plate. The mica plate was first immersed in the aqueous subphase; after spreading the monolayer, the film was compressed until the desired surface pressure and then deposited on the mica plate at the constant surface pressure. The speed of the transfer was 2 mm/min. We carried out AFM imaging in the noncontact mode with a commercial instrument Autoprobe CP (Park Scientific) fitted with a 2-μm cantilever (ultralever UL20) and a silicon monocrystalline tip. The scanning rate was 1 Hz.

Results and discussion

State of the spread films

The $\pi(A)$ and $\Delta V(A)$ isotherms for all pulmonary surfactant solutions were recorded. Usually, for such complex mixtures, the areas are expressed per mass of spread material ($m^2.mg^{-1}$). In order to compare these results with those previously obtained at 22 °C for model lipid and lipid–protein systems, we prefer to express the apparent areas per molecule DPPC, considering the real complex mixture with main component DPPC as a pure DPPC.

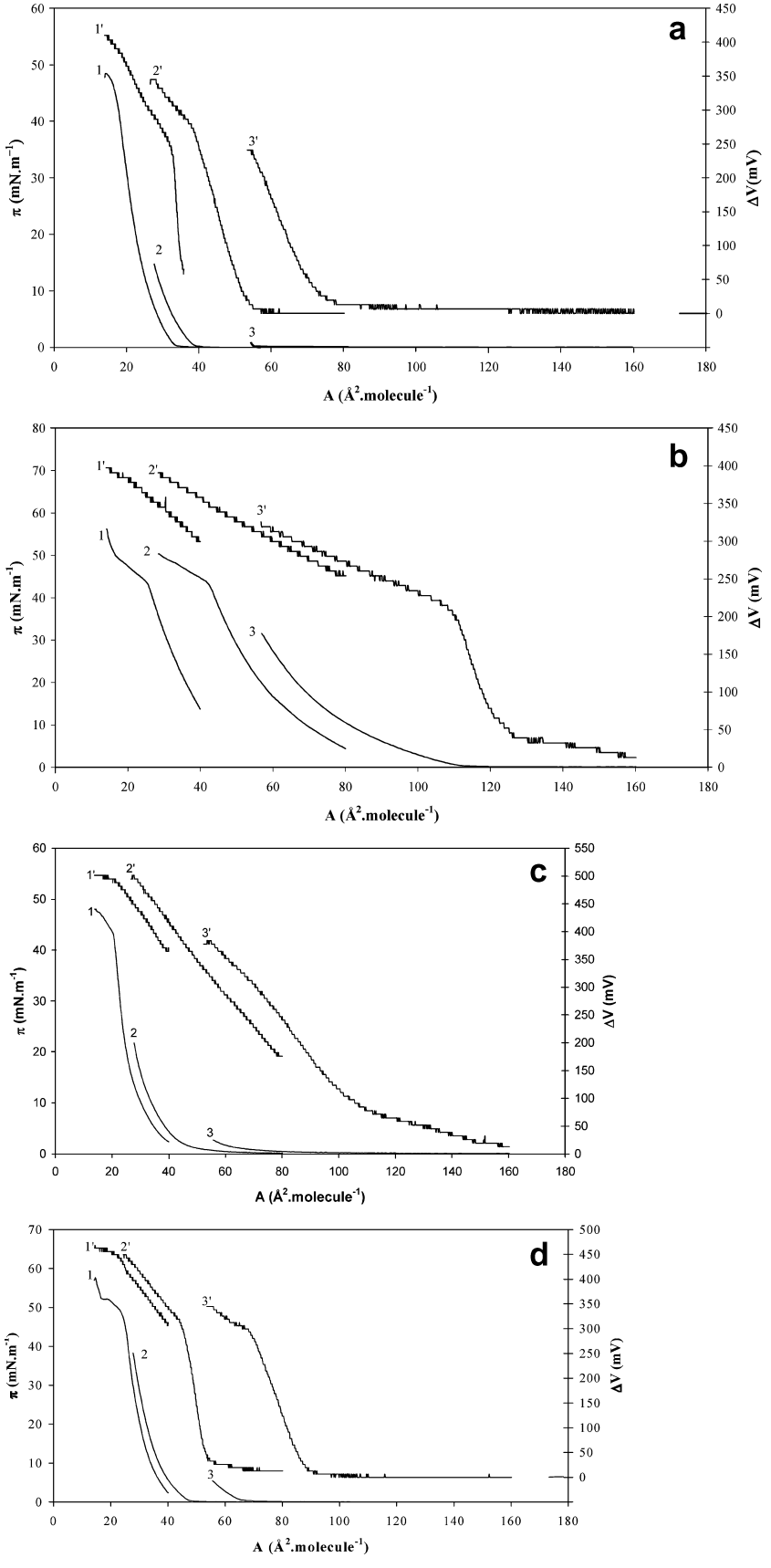

Fig. 2a–d Surface pressure (π)–area (A) (*curves 1*, *2*, *and 3*) and surface potential (ΔV)–area (A) (*curves 1′*, *2′*, *and 3′*) isotherms for different initially spread quantities of Alveofact (**a**), Curosurf (**b**), Exosurf (**c**), and Survanta (**d**). Initial mean areas per molecule: *curves 1 and 1′*, 40 Å^2.molecule^{-1}; *curves 2 and 2′*, 80 Å^2.molecule^{-1}; *curves 3 and 3′*, 160 Å^2.molecule^{-1}

In Fig. 2a the isotherms $\pi(A)$ (curves 1, 2, and 3) and $\Delta V(A)$ (curves 1′, 2′, and 3′) obtained after deposition of three different quantities of Alveofact (with initial apparent areas of 40, 80, and 160 Å^2 per molecule DPPC, respectively) are presented. It is obvious that the isotherms depend on the deposited quantity. A state close to a 2D monolayer organization can be considered when a small quantity at 160 Å^2 per molecule is spread. In fact, a dilute monolayer is initially formed and the ΔV potential values start from zero. When a large quantity at 40 Å^2 per molecule is spread, a more condensed layer is initially formed. A shift to the left of the isotherms is observed when larger quantities are deposited in comparison with the case where the compression starts from a more diluted initial state. This behavior may be due to the presence of nonspread 3D aggregates in the surface film. The presence of such aggregates can be confirmed by AFM imaging.

Similar results are obtained for all the pulmonary surfactants studied (Fig. 2b, c, and d). The isotherms obtained at 80 Å^2 per molecule show an intermediate behavior close to a quasi-2D monolayer organization especially for Alveofact and Survanta.

The isotherms of the studied pulmonary surfactant monolayers in the quasi-2D monolayer organization, obtained after spreading at 80 Å^2 per molecule (curves 1, 2, 3, and 4 in Figs. 3 and 4), are compared with each other and also with isotherms of the model lipid–protein monolayers DPPC/SP-B (Fig. 3) [29, 30, 31] and DPPC:DPPG:C–75:10:15 mol%/SP-C (Fig. 4) [17]. The shift of the isotherm of Curosurf to the right indicates better spreading and formation of a more expanded monolayer in comparison with the other three surfactants. Note that the areas calculated with the assumption that all spread material is constituted by DPPC molecules could be shifted variously because of the different composition of the studied surfactants. This circumstance sophisticates the comparison with model lipid–protein monolayers. Nevertheless the isotherms of the four pulmonary surfactants studied correspond reasonably to the behavior of a mixed lipid–protein monolayer between the isotherms of pure lipid (curve 5 in Figs. 3 and 4) and pure protein SP-B (curve 11 in Fig. 3) or SP-C (curve 9 in Fig. 4) monolayers.

The isotherms of the four surfactants can be compared without any restrictive assumption about the composition with the isotherm of the lipid fraction of total lung extract previously obtained [22]. The isotherms presented in Fig. 5 confirm the better spreading

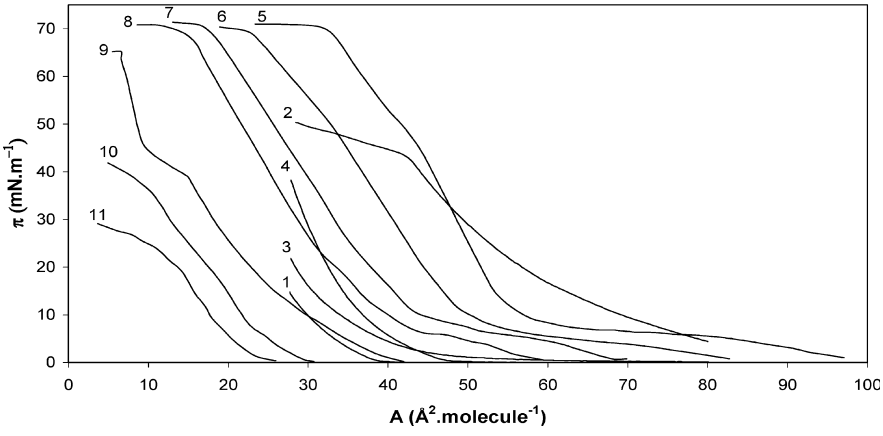

Fig. 3 Surface pressure (π)–area (A) isotherms of studied surfactants in comparison with the isotherms of model mixed lipid/protein monolayers. *Curve 1*, Alveofact; *curve 2*, Curosurf; *curve 3*, Exosurf; *curve 4*, Survanta. *Curves 5–11*, DPPC/SP-B with different protein mole (residual) fractions X_p: *Curve 5*, $X_p = 0$ (pure lipid DPPC); *curve 6*, $X_p = 0.29$; *curve 7*, $X_p = 0.49$; *curve 8*, $X_p = 0.57$; *curve 9*, $X_p = 0.80$; *curve 10*, $X_p = 0.92$; *curve 11*, $X_p = 1$ (pure protein SP-B)

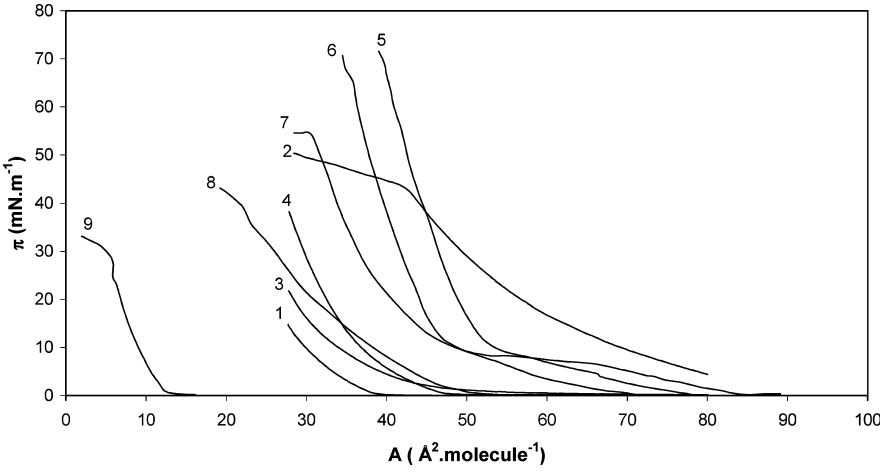

Fig. 4 Surface pressure (π)–area (A) isotherms of studied surfactants in comparison with the isotherms of model mixed lipid/protein monolayers L3/SP-C, where L3 is DPPC:DPPG:C–75:10:15 mol%. *Curve 1*, Alveofact; *curve 2*, Curosurf; *curve 3*, Exosurf; *curve 4*, Survanta. *Curves 5–9*, L3/SP-C with different protein mole (residual) fractions X_p: *Curve 5*, $X_p = 0$ (pure lipid mixture L3); *curve 6*, $X_p = 0.055$; *curve 7*, $X_p = 0.42$; *curve 8*, $X_p = 0.8$; *curve 9*, $X_p = 1$ (pure protein SP-C)

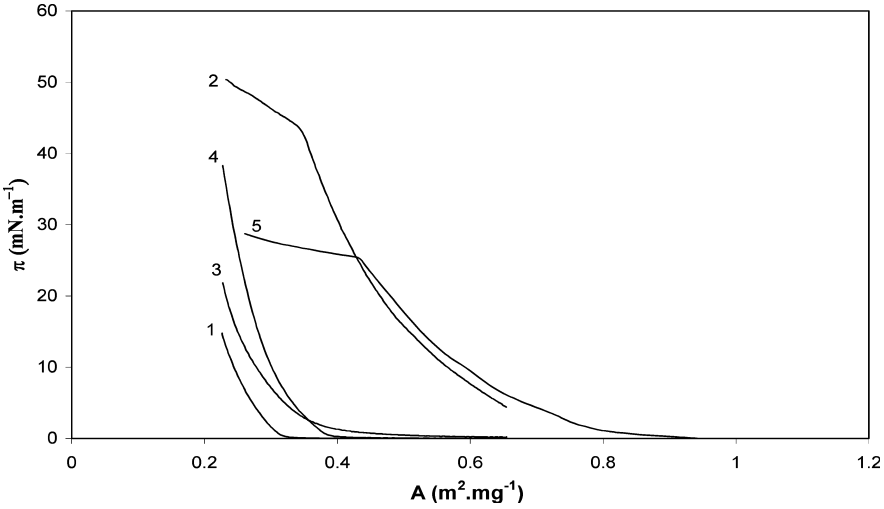

Fig. 5 Surface pressure (π)–area (A) isotherms of studied surfactants in comparison with lipid fraction of total lung extract. *Curve 1*, Alveofact; *curve 2*, Curosurf; *curve 3*, Exosurf; *curve 4*, Survanta; *curve 5*, lipid fraction of total lung extract [22]

and more expanded monolayer formed by Curosurf in comparison with the more condensed monolayers of Survanta, Exosurf, and Alveofact.

Dilatational properties

The dilatational strains are dominant over shear strains at the alveolar surface during respiration. Therefore, a study of the dilatational properties of model monolayers of the main lipid and nonlipid compounds as well as pulmonary surfactant monolayers seems indispensable. In order to test the effectiveness of spreading and respreading of the pulmonary surfactants, it is convenient to measure the $\pi(A)$ hysteresis at large extensions and times of deformation [1, 9].

By way of illustration, the first large $\pi(A)$ hysteresis recorded with the four pulmonary surfactants studied spread at 40 $Å^2$ per molecule are presented in Fig. 6. The large hysteresis loops are related to the surface viscoelasticity, the solubility of soluble trace components, and mainly to the collapse and respreading of the DPPC with characteristic times commeasurable with the period T of the compression–expansion cycle. The quantitative theoretical analysis of such large $\pi(A)$ hysteresis far from equilibrium is difficult, because the involved physicochemical processes are nonlinear and the surfactant chemical composition is not well known.

The interfacial dilatational properties can be analyzed when small, well-defined deformations are applied at conditions close to normal breathing ($\Delta A/A \leq 10\%$ and time $T \approx 5$ s) [22]. The typical experimental results $\Delta\pi(x,t)$ obtained at low initial surface pressure $\pi \approx 5$ mN.m^{-1} far from the collapse during and after a small continuous compression are shown in Fig. 7. According to the rheological model from Fig. 1, an elastic behavior for all studied surfactant layers is observed during the compression. The data for the dynamic elasticity ($E_e + E_{ne}$) were calculated in accordance

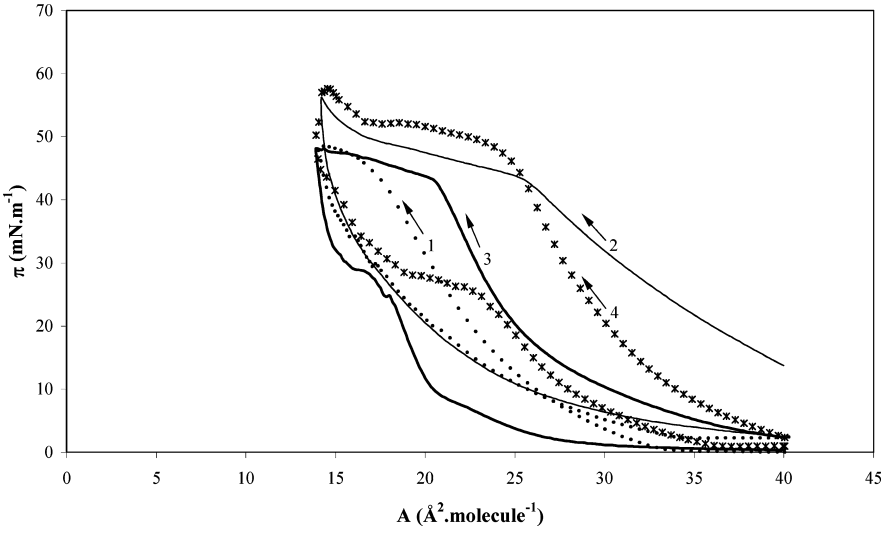

Fig. 6 Surface pressure (π)–area (A) large hysteresis for the studied surfactants. The initial mean area is 40 $Å^2$.molecule^{-1}. *Curve 1*, Alveofact; *curve 2*, Curosurf; *curve 3*, Exosurf; *curve 4*, Survanta

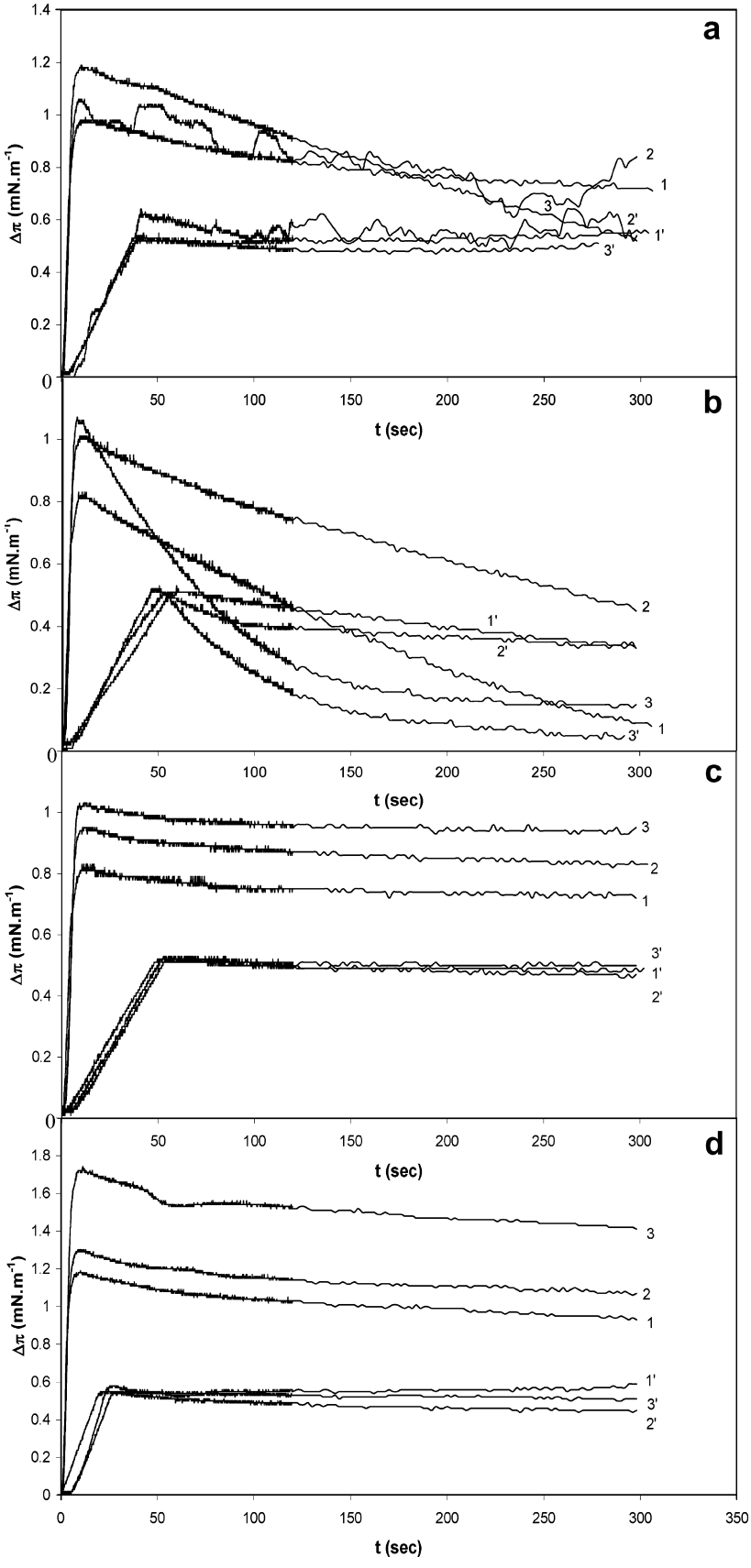

Fig. 7a–d Surface pressure change, $\Delta\pi$, with time t at various distances x (*curves 1 and 1′*, $x \approx 14$ cm; *curves 2 and 2′*, $x \approx 25$ cm; *curves 3 and 3′*, $x \approx 40$ cm) during a compression with two different velocities $U_b = 180$ cm^2.min^{-1} (*curves 1, 2, and 3*) and $U_b = 10$ cm^2.min^{-1} (*curves 1′*, *2′*, *and 3′*), and the consecutive relaxation of surfactant monolayers. **a** Alveofact, **b** Curosurf, **c** Exosurf, **d** Survanta

with Eq. 5 and are presented in Table 1. After stopping the compression, the relaxation processes with characteristic time τ are observed, i.e., viscoelastic behavior. The equilibrium $\Delta\pi_e$ and nonequilibrium $\Delta\pi_{ne}$ parts of the total surface pressure change $\Delta\pi$ and the specific time of relaxation τ were calculated by using Eq. 6 and are also presented in Table 1. The nonequilibrium effects due to the reorganization of the molecules with a characteristic time of about 100 s are important for Curosurf and Alveofact (~90 and ~40%, respectively) and related to a better effectiveness of spreading of the 3D aggregates. Exosurf and Survanta show a quasielastic behavior with $\tau \gg 100$ s.

The data $\Delta\pi(x,t)$ (not shown) obtained at higher surface pressures close to the collapse show the more pronounced nonequilibrium effects. Unfortunately, analysis on the basis of the proposed rheological model is difficult because the monolayers are unstable and the initial high surface pressure π_i decreases rapidly.

Morphology of surface films by AFM imaging after LB transfer

AFM imaging of the four pulmonary surfactant monolayers at three surface pressures, corresponding to the $\pi(A)$ hysteresis curves obtained after spreading at 40 Å^2 per molecule, was carried out:

(i) At low surface pressures $\pi \approx 5$ mN.m^{-1} before the compression–expansion cycle.
(ii) At high surface pressures $\pi \approx 40$ mN.m^{-1} close to the collapse.
(iii) At low surface pressures $\pi \approx 5$ mN.m^{-1} after the large compression–expansion hysteresis cycle.

AFM images are presented in Fig. 8.

Alveofact

(i) At low surface pressure the segregated zones formed by lipid molecules with different chain lengths are presented. The observed overheight is about 6–8 Å (Fig. 8a).
(ii) At the collapse, a coalescence of the zones with overheight of about 6–8 Å is observed. The white points are the collapsed protein phases with overheight of 26 Å with respect to the light zone (Fig. 8b).
(iii) The respreading after expansion is perfect and the aggregates disappear completely (Fig. 8c).

Curosurf

(i) Two domains with overheight between them of about 12 Å are observed (Fig. 8d).
(ii) At high surface pressure populations of big and small aggregates are observed. The background was homogeneous. The overheight between the small aggregates and the background is about 18 Å, and between the big ones and the background, 263 Å. The big aggregates are probably protein collapsed phases (Fig. 8e).
(iii) After the compression–expansion cycle, there is a small number of small and big aggregates with overheights 5 and 118 Å, respectively (Fig. 8f).

Exosurf

(i) The overheight between the bright and dark areas is estimated to be around 10 Å. A typical fractality for the phospholipid layers is observed (the appearance of holes may be related to drying on the mica plate) (Fig. 8g).
(ii) The fractality of the structures increases and three-dimensional aggregates of the collapsed lipid material with overheight around 80 Å are observed (Fig. 8h).
(iii) After the large hysteresis loop the results are similar to those at low surface pressure. The overheight between the light and dark zones is around 5 Å. The holes are larger than those at the beginning of the compression (Fig. 8i).

Table 1 Dynamic elasticity ($E_e + E_{ne}$), equilibrium $\Delta\pi_e$, and non-equilibrium $\Delta\pi_{ne}$ parts of the total surface pressure change $\Delta\pi$ and the specific time of relaxation τ for pulmonary surfactant surface layers

Alveofact					Curosurf			
x (cm)	$\Delta\pi_e$ (%)	$\Delta\pi_{ne}$ (%)	τ (s)	E_e+E_{ne} (mN.m^{-1})	$\Delta\pi_e$ (%)	$\Delta\pi_{ne}$ (%)	τ (s)	E_e+E_{ne} (mN.m^{-1})
15	61.1	38.9	108.1	32.1	9.7	90.3	118.1	26.1
24	76.0	24.0	53.6	30.5	41.5	58.5	144.8	32.3
40	59.4	40.6	124.3	38.3	7.2	92.8	67.9	29.3
Exosurf					Survanta			
x	$\Delta\pi_e$	$\Delta\pi_{ne}$	τ	E_e+E_{ne}	$\Delta\pi_e$	$\Delta\pi_{ne}$	τ	E_e+E_{ne}
15	86.9	13.1	$\gg 100$	27.9	78.2	21.8	$\gg 100$	68.9
24	85.7	14.3	$\gg 100$	27.8	82.4	17.6	$\gg 100$	58.2
40	89.3	10.7	$\gg 100$	25.0	79.2	20.8	$\gg 100$	69.4

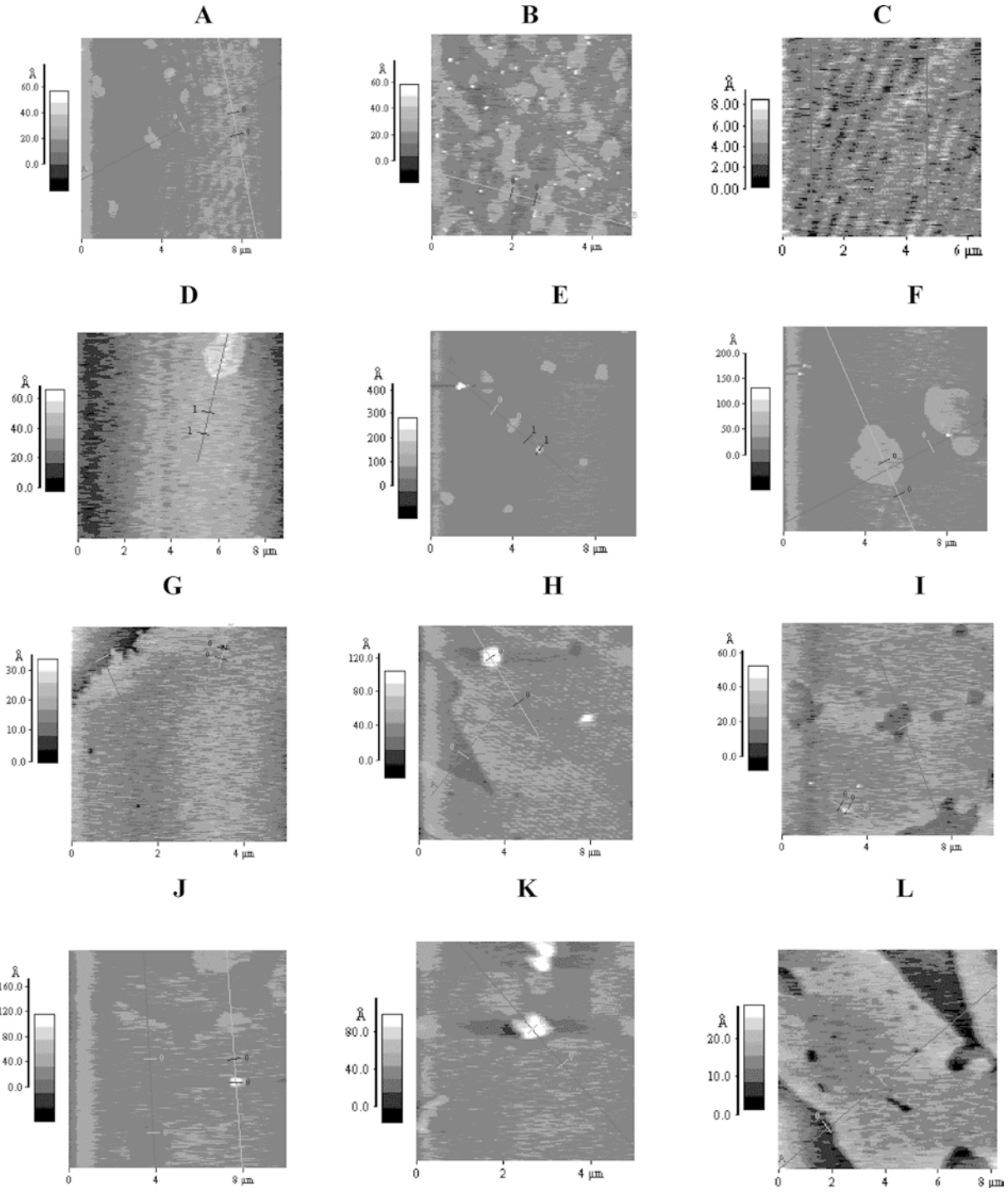

Fig. 8a–l AFM imaging for the four pulmonary surfactant monolayers (**a–c** Alveofact; **d–f** Curosurf; **g–i** Exosurf; **j–l** Survanta) at three surface pressures: (i) at low surface pressures $\pi \approx 5$ mN.m^{-1} before the compression–expansion cycle (**a**, **d**, **g**, and **j**); (ii) at high surface pressures $\pi \approx 40$ mN.m^{-1} close to the collapse (**b**, **e**, **h**, and **k**); (iii) at low surface pressures $\pi \approx 5$ mN.m^{-1} after the large compression–expansion hysteresis cycle (**c**, **f**, **i**, and **l**)

Survanta

(i) Two domains, light gray and dark gray, with overheight between them of 10 Å are observed. In spite of a relatively low pressure $\pi \approx 6$ mN.m^{-1}, white protein aggregates with overheight about 90 Å are also present (Fig. 8j).

(ii) Close to the collapse, the overheight between the light protein aggregates and a more homogeneous light gray domain is about 53 Å (Fig. 8k).
(iii) Two domains (a light and a dark one) are observed as at the beginning of the compression but the protein aggregates disappear. Probably the protein molecules are closely linked with the lipid ones in the layer (Fig. 8l).

Similar structures were recently observed [32]. Below the collapse, the images consist of distinct domains with overheight between them of 10 Å, corresponding to the coexistence of condensed and fluid-phase monolayers. The formation of white patches above the plateau pressure with overheight of 50–80 Å is observed. The presence of such patches, called ''nanosilos'', may be related to a mechanism of stabilizing the unsaturated lipids and SP-B in 3D aggregates for subsequent reincorporation as the monolayers are expanded.

In conclusion, the spread films of the natural surfactants Curosurf and Alveofact show a high effectiveness of spreading and respreading. After the compression–expansion hysteresis loop, there are fewer aggregates than at the collapse and the morphology of the films is similar to that before compression. In the films formed from Exosurf and Survanta, the respreading is less effective and after the hysteresis loop the aggregates and condensed phases partially remain.

Acknowledgment The authors acknowledge financial support from the Foundation for Scientific Research of the University of Sofia (no. 682/2001); two of us Tz. Ivanova—the University of Angers and I. Panaiotov—INSERM (France).

References

1. Scarpelli EM (1998) Surfactants and the lining of the lung. Johns Hopkins University Press, Baltimore and London
2. Notter RH (1988) Semin Perinatol 12:180
3. Possmayer F (1984) In: Robertson B, van Golde LMG, Batenburg JJ (eds) Pulmonary surfactant. Elsevier, Amsterdam, p 295
4. King RJ (1984) In: Robertson B, van Golde LMG, Batenburg JJ (eds) Pulmonary surfactant. Elsevier, Amsterdam, p 1
5. Hawgoold S (1989) Am J Physiol 257:L13
6. Suzuki Y, Kogishi K, Fujita Y (1990) In: von Wichert P, Muller B (eds) Basic research on lung surfactant. Karger, Basel, p 91
7. Oosterlaken-Dijksterhuis MA, van Eijk M, van Buel BLM, van Golde LMG, Haagsman HP (1991) Biochem J 274:115
8. Possmayer F, Cockshutt A, Yu SH (1990) In: Cosmi GC, Di Renzo GC, Anchesni MM (eds) The surfactant system of the lung. McMillan, London, pp 7–17
9. Nottrer RH (2000) Lung surfactants: basic science and clinical applications, vol 149. Marcel Dekker, New York
10. Bernhard W, Mottaghian J, Gebert A, Rau GA, von der Hardt H, Poets CF (2000) Am J Respir Crit Care Med 162:1524
11. Goerke J (1998) Biochim Biophys Acta 1408:79–89
12. Avery ME (1959) Am J Dis Child 97:517
13. Simatos GA, Forward KB, Morrow MR, Keough KMW (1990) Biochem 29:5807
14. Keough KMW, Simatos G, Perez-Gil J, Nag K, Allwood LA, Morrow MR (1992) Thin Solid Films 210/211:720–722
15. Yu F, Possmayer SH (1992) Biochim Biophys Acta 1126:26
16. Creuwels LAJM, van Golde LMG, Hagsman HP (1997) Lung 175:1
17. Panaiotov I, Ivanova Tz, Proust J, Boury F, Denizot B, Keough K, Taneva S (1996) Colloids Surf B Biointerfaces 6:243
18. Mutafchieva R, Panaiotov I, Dimitrov DS (1984) Z Naturforsch C 39:965
19. Ueno M, Samura K, Fukuda K, Takeo N, Takei T, Takahashi A, Fujiwara T, Asano H (1993) Colloids Surf B Biointerfaces 1:221
20. Sasaki M, Iwate J (1990) Med Ass 42:883
21. Banerjee R, Bellare JR (2002) Int J Aromatherapy 12(1):40
22. Panaiotov I (1987) Thesis, University of Sofia
23. Dimitrov D, Panaiotov I (1975/76) Ann Univ Sofia Fac Chem 70:103
24. Dimitrov D, Panaiotov I, Richmond P, Ter-Minassian-Saraga L (1978) J Colloid Interface Sci 65:483
25. Panaiotov I, Dimitrov DS, Ter-Minassian-Saraga L (1979) J Colloid Interface Sci 72:49
26. Panaiotov I, Dimitrov DS, Ivanova (1979) J Colloid Interface Sci 69:318
27. Panaiotov I, Sanfeld A, Bois A, Baret J F (1983) J Colloid Interface Sci 96:315
28. Loglio G, Tesej U, Miller R (1991) Colloids Surf 61:219
29. Taneva S, Keough KMW (1994) Biophys J 66:1137
30. Taneva S, Keough KMW (1994) Biophys J 66:1149
31. Taneva S, Keough KMW (1994) Biophys J 66:1158
32. Ding J, Doudevski I, Warriner HE, Alig T, Lasadzinski J, Waring A, Sherman M (2003) Langmuir 19(5):1539–1550